EXOSKELETONS

Individualization of exosuit assistance based on measured muscle dynamics during versatile walking

R. W. Nuckols*†, S. Lee†, K. Swaminathan†, D. Orzel, R. D. Howe, C. J. Walsh*

Variability in human walking depends on individual physiology, environment, and walking task. Consequently, in the field of wearable robotics, there is a clear need for customizing assistance to the user and task. Here, we developed a muscle-based assistance (MBA) strategy wherein exosuit assistance was derived from direct measurements of individuals' muscle dynamics during specific tasks. We recorded individuals' soleus muscle dynamics using ultrasonographic imaging during multiple walking speeds and inclines. From these prerecorded images, we estimated the force produced by the soleus through inefficient concentric contraction and designed the exosuit assistance profile to be proportional to that estimated force. We evaluated this approach with a bilateral ankle exosuit at each measured walking task. Compared with not wearing a device, the MBA ankle exosuit significantly reduced metabolic demand by an average of 15.9, 9.7, and 8.9% for level walking at 1.25, 1.5, and 1.75 meters second^{-1}, respectively, and 7.8% at 1.25 meters second^{-1} at 5.71° incline while applying lower assistance levels than in existing literature. In an additional study ($n = 2$), we showed for multiple walking tasks that the MBA profile outperforms other bioinspired strategies and the average profile from a previous optimization study. Last, we show the feasibility of online assistance generation in a mobile version for overground outdoor walking. This muscle-based approach enables relatively rapid (~10 seconds) generation of individualized low-force assistance profiles that provide metabolic benefit. This approach may help support the adoption of wearable robotics in real-world, dynamic locomotor tasks by enabling comfortable, tailored, and adaptive assistance.

INTRODUCTION

Wearable robotic systems have the potential for assisting locomotion in numerous areas, including recreation, clinical rehabilitation and assistance, and occupations with demanding tasks. As the field moves toward designing for more widespread use and real-world applications, the effectiveness of systems will depend on their ability to address variability in the human user and to adapt to different tasks. Human walking is influenced by sex, height, body composition, age, and muscle strength (*1*–*6*) and can be further affected by neural or muscular disorders such as stroke (*7*) or Parkinson's disease (*8*). An individual's walking is also altered by the environment (*9*–*11*) and task (*12*–*14*).

The importance of human individuality and the need for customizing exoskeleton or exosuit assistance to the person and task are becoming increasingly clear in the field of wearable robotics. For the lower extremity, the leading approach for individualizing assistance profiles to the person is human-in-the-loop (HIL) optimization (*15*). By continuously measuring physiologic feedback of whole-body metabolic demand while individuals walk with assistance, the assistance profiles and parameters can be iteratively updated until metabolic demand is minimized. This approach has produced exciting results, significantly reducing the energy cost of walking (*15*, *16*) and running (*17*). However, although optimization is effective, it also requires a relatively long time (64 to 208 min) to converge on optimal parameters for even a single walking task (e.g., fixed speed and level ground) (*15*).

An alternative approach for assistance derives the profiles from biological mechanisms and aims to mimic the intent of the individual at a local joint or muscle level. By emulating the mechanics of the wearer, these biomechanistic strategies may enable increased versatility because the assistance is inherently reflective of the individual and how they adapt to locomotor tasks. Prior joint-level approaches have targeted joint moment, power, or key features of them (e.g., onset, peak, and offset timings of assistance) (*18*–*22*). Proportional surface electromyography (EMG)–based controllers measure the neural activation of a muscle and generate assistance profiles that are proportional to that neural activation profile (*23*, *24*). Studies using these biomechanistic approaches have shown that assisting specific muscles can lead to reductions in whole-body energetics and, at a local level, reduce biological joint moment, power, and muscle activity (*18*–*20*, *23*). Despite existing mechanistic approaches having benefits of individualization and adaptability, a limitation may be that they do not fully consider the underlying muscle-tendon (MT) dynamics (Fig. 1A), which cannot be entirely captured with conventional kinematic or EMG measurement techniques (*25*, *26*).

The ability of the ankle joint to efficiently produce the majority of positive power in walking (*26*) is linked to the ankle plantar flexor MTs. Over a gait cycle, the plantar flexor MTs with short pennate muscle fascicles and long compliant in-series tendons enable efficient storage and return of elastic mechanical energy (*27*). The neuromuscular system is tuned to permit this effective exchange of energy between the muscle, tendon, and environment. In level walking at 1.25 m s^{-1}, during early stance (~0 to 30% of the gait cycle), the plantar flexor muscle fascicles generate force approximately isometrically, meaning that the muscle is not changing length and is acting like a mechanical clutch. By remaining approximately isometric, the muscle fascicle can operate under favorable force-velocity (F-V) contractile conditions where force production is economical (Fig. 1B). During this time region, the Achilles tendon (AT) is also stretching and storing mechanical energy while the ankle dorsiflexes. Toward mid-stance (~40%), the muscle begins to contract concentrically (shorten) to add additional energy to the MT system.

John A. Paulson School of Engineering and Applied Sciences and Wyss Institute for Biologically Inspired Engineering, Harvard University, Boston, MA, USA.
*Corresponding author. Email: rnuckols@seas.harvard.edu (R.W.N.); walsh@seas.harvard.edu (C.J.W.)
†These authors contributed equally to this work.

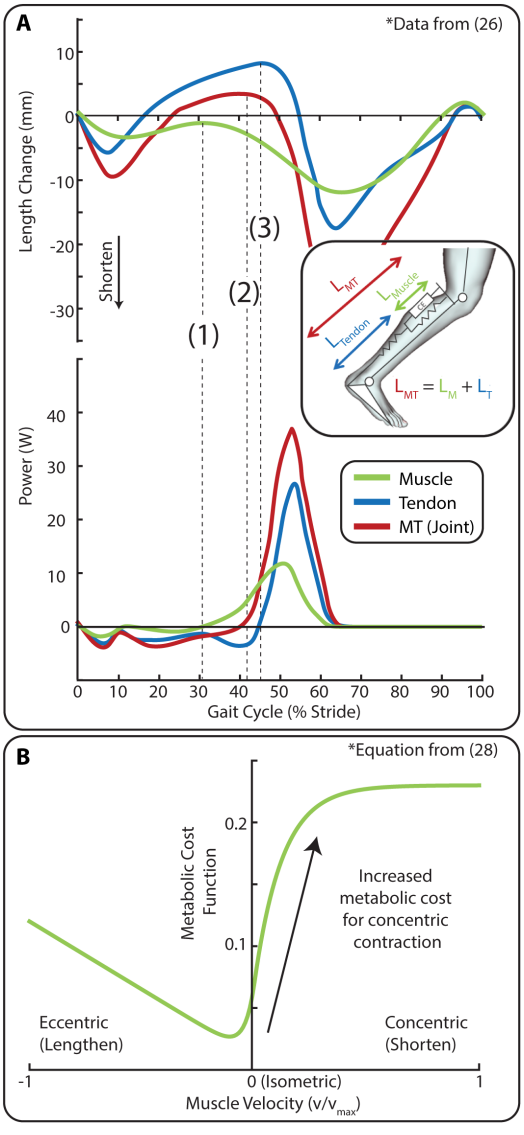

Fig. 1. Ankle MT mechanics and energetics. (**A**) Example of length change and power of the muscle fascicle, tendon, and MT (ankle joint) for fast walking [figure created from data from (*26*)]. Between heel strike (0%) and (1), the muscle remains approximately isometric/eccentric, the ankle is dorsiflexing, which elongates the MT, and the tendon stores mechanical elastic energy. At (1), muscle concentric contraction begins, and the muscle produces positive power. Mechanical energy continues to be stored in the tendon. At (2), the ankle begins plantar flexion rotation and produces positive joint (MT) power. Shortly after at (3), the tendon returns the mechanical energy, resulting in a burst of positive power at the ankle. (**B**) Isometric and eccentric muscle contractions are more efficient than concentric contractions [Equation from (*28*)]. The muscle-based assistance profile is designed to selectively target the region of concentric contraction [(1) to toe-off] where the muscle is less efficient.

Last, during late stance (~40 to 60%), the muscle continues to contract concentrically to generate additional positive power, and the energy that was stored in the tendon is returned to generate positive power for push-off. The production of force during concentric contraction is understood to be more metabolically costly than eccentric or isometric contraction due to reduced mechanochemical efficiency of adenosine 5′-triphosphate synthesis (*28*–*30*).

These timings are average approximations for level walking at 1.25 m s^{-1}, but MT dynamics vary across individuals and are task dependent (*31*, *32*). As walking speed changes, fascicle shortening velocity changes to accommodate the demands (*26*, *33*). For uphill walking, positive power is needed to raise the center of mass; however, the relatively high compliance of the ankle MT makes it less effective in these tasks (*34*, *35*). By understanding how individuals take advantage of MT mechanisms to produce efficient movement in a variety of activities, we have the opportunity to develop systems that work more synergistically with the user. We expect that an exosuit assistance strategy based on the individuals' measured muscle dynamics (i.e., force and power) in the specific task would improve exosuit performance and provide benefit during real-world use.

We developed a muscle-based assistance (MBA) strategy wherein the exosuit assistance was derived from direct measurements of soleus muscle dynamics from each participant as they walked in multiple walking tasks. We directly measured soleus muscle dynamics by using brightness-mode (B-mode) ultrasonography, which captured a continuous sequence of two-dimensional images of the soleus as participants walked. For each individual and task, we prerecorded B-mode ultrasound images and estimated the force produced by the soleus during the inefficient concentric contraction phase. We then designed the exosuit assistance profile to be proportional to that estimated force. This approach allowed us to separate the force generation developed through efficient passive tendon mechanics and economical isometric muscle contraction from the force that is generated uneconomically when the muscle concentrically contracts (i.e., shortening and producing positive power). We focus only on the soleus muscle because it is the largest of the plantar flexor muscles, making up about 54% of the physiological area (*36*). This was done to simplify the approach and to aim for the lowest level of force that provides appreciable benefit.

We developed and tested the MBA approach with a bilateral ankle soft exosuit at multiple walking speeds (1.0, 1.25, 1.5, and 1.75 m s^{-1}) and incline walking (1.25 m s^{-1} at a 5.71° incline). Our goal was to assess whether the bilateral ankle assistance with the MBA profile would be effective in reducing the metabolic energy demand for these walking tasks compared with not wearing a device. To further reinforce our investigation into the effectiveness of the MBA profile, we performed an additional study that directly compared the MBA profile with other bioinspired strategies and the average profile from a previous optimization study with high assistance levels (*15*, *37*). We also performed a single-participant study where we used ultrasonography to directly measure the effects of MBA assistance on muscle dynamics. Last, we performed a proof-of-concept study demonstrating the feasibility of online MBA assistance generation in a mobile ankle exosuit for overground outdoor walking.

RESULTS

Muscle dynamics–based assistance profile generation

We acquired B-mode ultrasound images, joint kinematics and kinetics, and EMG on 9 healthy adults [n = 9, 3 females and 6 males; age = 29.1 ± 4.04 years (means ± SD); mass = 67.9 ± 12.9 kg; height = 1.71 ± 0.07 m] while they walked at speeds of 1.0, 1.25, 1.5, and 1.75 m s^{-1} on level ground and additionally at 1.25 m s^{-1} at a 5.71° (10% grade) incline. From these data, we calculated the task-specific assistance profiles for each participant that were designed to mimic the demand for concentric contraction in the muscle (Fig. 2 and fig. S1).

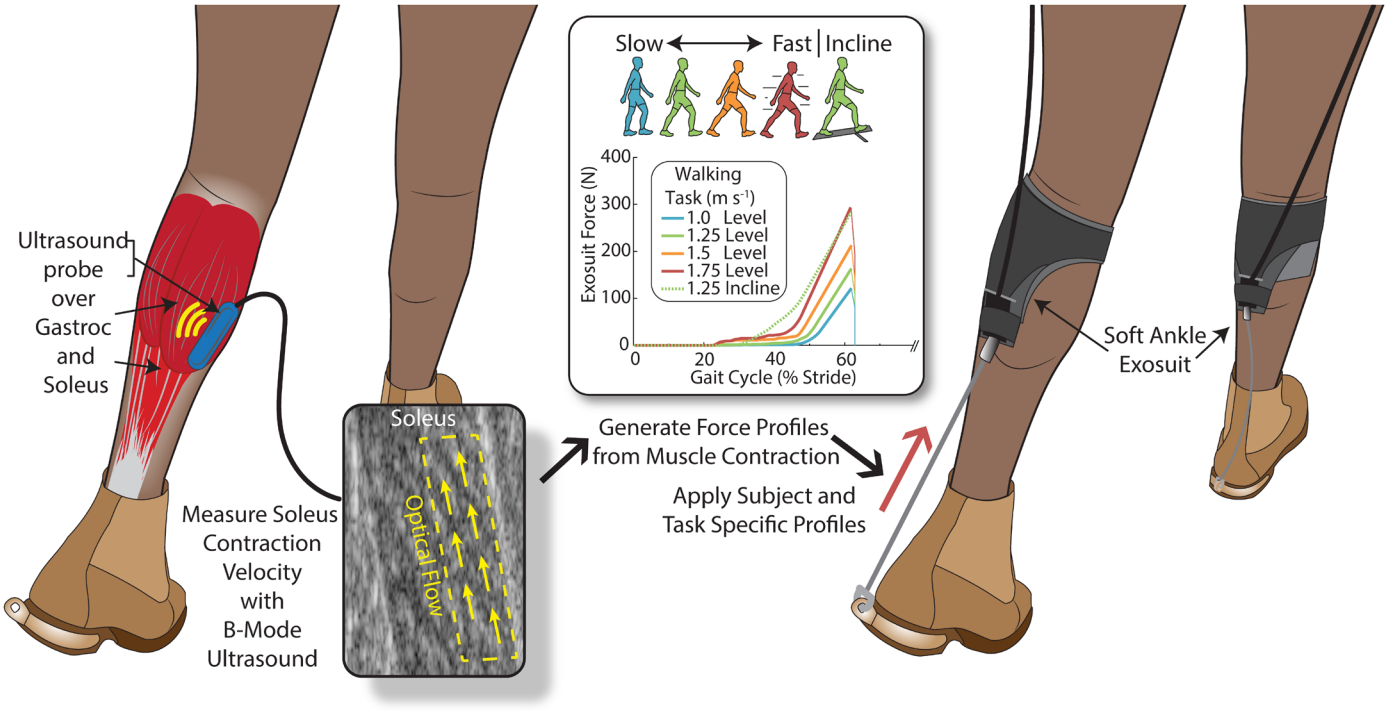

Fig. 2. Generation of the MBA profile from measured soleus dynamics. A low-profile ultrasound probe recorded images of the soleus while participants walked in multiple tasks. We performed offline optical flow image processing to measure the velocity of the muscle concentric contraction. From this velocity profile, we estimated the stretch generated in the tendon and, by multiplying by tendon quasi-stiffness, the force in the tendon generated by muscle concentric contraction. These unique profiles were applied back to the participants through the ankle exosuit to offset the requirement of the soleus to produce positive power and reduce energy use.

As level ground walking speed increased, the exosuit profiles exhibited earlier force development and higher force magnitude. Similarly, compared with level walking, uphill walking profiles at matched speed developed force earlier and had higher force magnitude (Fig. 3A, fig. S2, and table S1).

To highlight the importance of evaluating the underlying muscle in developing individual and task-specific profiles, we analyzed how the joint and the estimated muscle dynamics changed across conditions and participants. The response to changing tasks varied more in the muscle than at the joint. Compared with level 1.25 m s^{-1}, MBA force at 60% of the gait cycle changed by −39.4, 61.3, 121.2, and 99.9% for 1.0, 1.5, and 1.75 m s^{-1} and 5.71° incline (Fig. 3A, fig. S2, and table S1). There was a slight negative but nonsignificant correlation between peak MBA exosuit torque (non–mass normalized) and body mass [two-way analysis of variance (ANOVA); main effect: mass, $P = 0.2409$; task, $P < 0.0001$; coefficient of determination (R^2) = 0.56]. The ankle joint produced relatively similar moments across walking speeds and inclines and was similar across participants. Compared with level 1.25 m s^{-1}, peak ankle joint moment changed by −9.3, 8.7, 17.2, and 13.1% for 1.0, 1.5, and 1.75 m s^{-1} and 5.71° incline. Peak ankle power was more sensitive across walking speeds with a difference of −29.2, 26.1, and 54.2% for 1.0, 1.5, and 1.75 m s^{-1} compared with 1.25 m s^{-1} but was less sensitive to incline, which increased by 19.5% for 5.71° (Fig. 3A, fig. S2, and table S2). Moreover, the onset of positive muscle power was more sensitive to the walking task than the onset of positive joint power (table S1).

Effect of MBA profile on metabolic demand in multiple walking tasks

We tested whether the MBA method was effective at reducing metabolic energy demand. After a training session, the nine participants walked in the same walking tasks, with the ankle exosuit applying plantar flexion (PF) assistance using the individualized and task-specific MBA profiles (Fig. 3B). The peak applied torque was 0.18 ± 0.03, 0.23 ± 0.03, 0.30 ± 0.03, 0.33 ± 0.03, and 0.38 ± 0.03 N m kg^{-1} for 1.00, 1.25, 1.5, and 1.75 m s^{-1} and 5.71° walking, respectively (table S2). The MBA approach allowed us to develop assistance profiles that were effective across a range of walking tasks. Compared with NO-DEVICE, the exosuit with the MBA profiles significantly reduced the metabolic demand for level walking at 1.25, 1.5, and 1.75 m s^{-1} and for 5.71° incline walking at 1.25 m s^{-1}. The net metabolic reduction comparing MBA with NO-DEVICE for level walking was −0.70 ± 0.24 W kg^{-1} (means ± SEM) (Wilcoxon signed-rank, two-tailed, $n = 9$, $z = -22$; $P = 0.0078$; 15.9%) at 1.25 m s^{-1}, −0.53 ± 0.22 W kg^{-1} ($n = 9$, $z = -18.5$; $P = 0.0273$; 9.7%) at 1.5 m s^{-1}, −0.66 ± 0.26 W kg^{-1} ($n = 7$, $z = -12$; $P = 0.0469$; 8.9%) at 1.75 m s^{-1}, and −0.74 ± 0.32 W kg^{-1} ($n = 9$, $z = -19.5$; $P = 0.0195$; 7.8%) at 5.71° (Fig. 3C and table S3). We measured a slight nonsignificant reduction of −0.22 ± 0.22 W kg^{-1} ($n = 9$, $z = -5$; $P = 0.5859$; 4.3%) at 1.0 m s^{-1}. We calculated the efficiency of the exosuit force application [metabolic reduction per unit of applied peak torque (watt $newton^{-1}$ $meter^{-1}$)] by dividing the metabolic reduction (watt $kilogram^{-1}$) by peak applied torque (newton meter $kilogram^{-1}$). Compared with other assistance strategies reported in literature

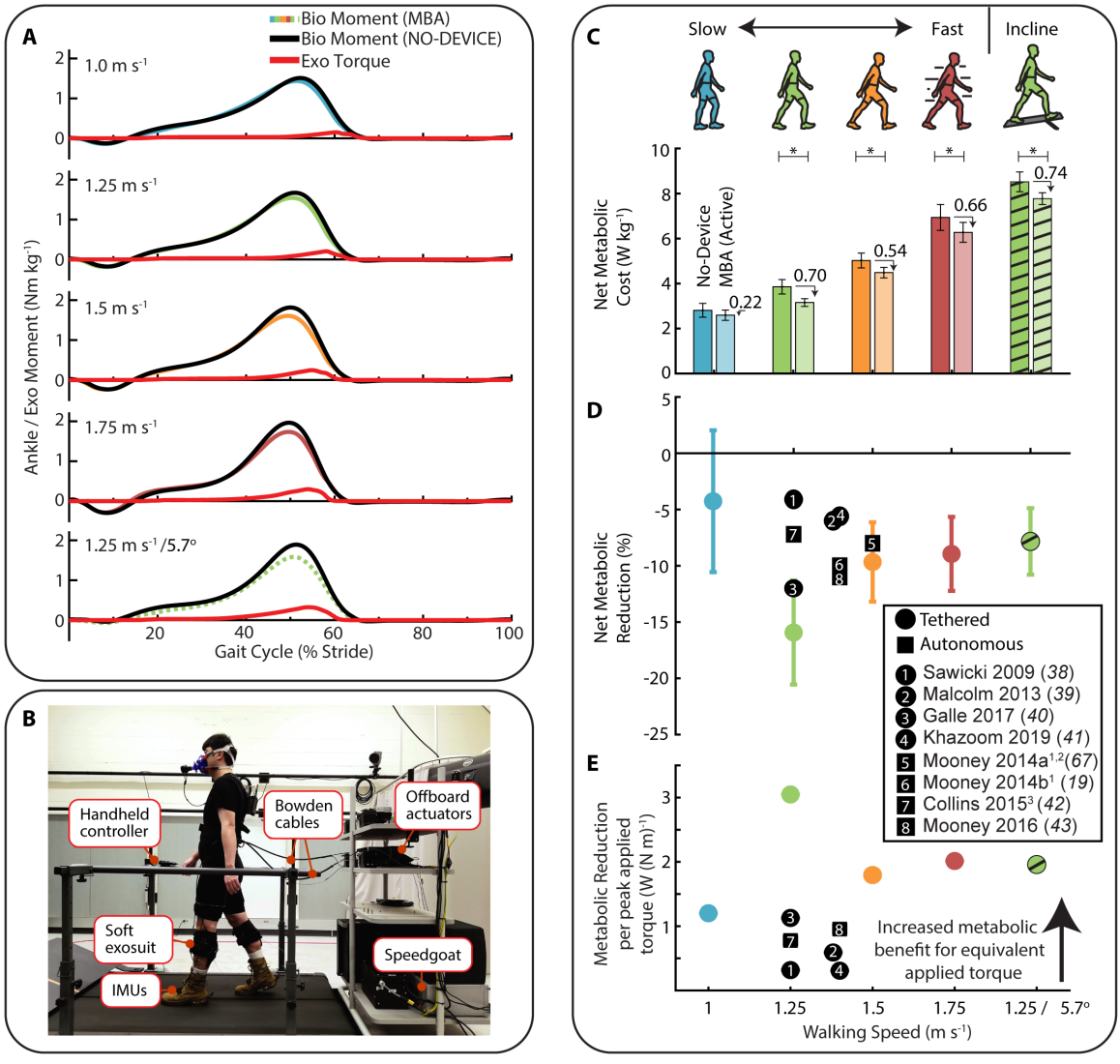

Fig. 3. Biomechanical and energetic response to the MBA ankle exosuit across a range of walking tasks. (**A**) Group average ankle moment and exosuit torque profiles for each walking task normalized by participant body mass MBA exosuit assistance resulted in lower biological ankle moments. (**B**) Ankle exosuit with offboard actuation for the main study. (**C**) Group average net metabolic energy (watts kilogram^{-1}; means ± SEM) use for each of the walking tasks (*$P < 0.05$). Energy use was lower with the MBA exosuit compared with NO-DEVICE for all except the slowest walking speed. (**D**) Metabolic reduction (%; means ± SEM) for each walking task relative to wearable ankle robots in literature that compared with NO-DEVICE (*19*, *38*–*43*, *67*). (**E**) The ratio of the metabolic reduction (watts kilogram^{-1}) to the applied ankle assistive torque (newton meter kilogram^{-1}). The MBA ankle exosuit had a higher metabolic benefit for equivalent applied torque. The torques estimated for the MBA profiles were generally lower than those used in other studies (fig. S7). (Notes: [1]Exoskeleton torque not reported; [2]Walking with load carriage; [3]Passive device; $n = 9$ for 1.0, 1.25, and 1.5 m s^{-1} and 5.71°; $n = 7$ for 1.75 m s^{-1}.)

(*38*–*43*), the MBA profile was also more efficient at reducing metabolic demand (Fig. 3E).

Effects of MBA profile on biomechanics

We evaluated the biomechanics of the ankle comparing the MBA profile with the NO-DEVICE condition in each walking task. Peak PF angle and velocity increased significantly for all walking tasks with MBA. Peak ankle dorsiflexion angle did not significantly change (fig. S3 and table S2).

Peak net (Bio + Exo) ankle moment did not change significantly in any of the walking tasks (Fig. 3A, figs. S2 and S3, and table S2). Peak biological component of ankle moment was reduced by 2.8% (two-tailed paired t test; $P = 0.1698$), 6.1% ($P = 0.0407$), 10.7% ($P = 0.0033$), 10.2% ($n = 6$, $P = 0.0385$), and 15.6% ($P < 0.0001$) for 1.0, 1.25, 1.5, and 1.75 m s^{-1} and 5.71° (figs. S2 and S3 and table S2). Peak biological positive power increased by 18.7% ($P = 0.0078$), 26.5% ($P = 0.0117$), 30.2% ($P = 0.0039$), 36.2% ($n = 6$, $P = 0.0313$), and 17.5% ($P = 0.0391$) (fig. S3 and table S2).

Average soleus activation during mid-late stance (20% stride to peak ankle torque) significantly decreased by 4.6% (two-tailed paired t test; $P = 0.0463$), 7.18% ($P = 0.0449$), 6.6% ($P = 0.0490$), 8.5% ($P = 0.0371$), and 9.2% ($P = 0.0493$) for 1.0, 1.25, 1.5, and 1.75 m s^{-1}

and 5.71° (fig. S3 and table S4). Peak soleus activation during stance decreased for the same conditions by 7.6, 8.7, 7.7, 7.4, and 7.7%, but the changes were not significant. Tibialis anterior (TA) activation did not increase with exosuit assistance and instead significantly decreased under the 1.25 m s^{-1} condition (n = 9, Wilcoxon signed-rank, two-tailed; P = 0.0117).

Evaluation of MBA profile against alternative assistance strategies

The four assistance profiles—MBA, muscle activation (EMG), joint power (POW), and fixed (FXD)—were evaluated for walking at 1.0, 1.25, and 1.75 m s^{-1} and 5.71° (Fig. 4A). We removed the 1.5 m s^{-1} task to maintain the range of tasks while keeping a reasonable session length. On average, across the four tasks, the metabolic demand with MBA was lower than with FXD, POW, and EMG profiles by 0.28 ± 0.15, 0.26 ± 0.15, and 1.09 ± 0.36 W kg^{-1} (means ± SD) (Fig. 4B). The peak applied forces for the POW and EMG profiles were set to the peaks of the MBA profiles, which were 170 ± 14, 229 ± 21, 329 ± 13, and 335 ± 16 N for 1.0, 1.25, and 1.75 m s^{-1} and 5.71°, to normalize the assistance levels. The peak applied force for the FXD profile was fixed on the basis of participant body mass per the approach in (*15*, *37*) and was 430 ± 20 N across the conditions. Across the walking tasks, the metabolic benefit for the given level of torque was higher with MBA compared with FXD, EMG, and POW (Fig. 4C).

Evaluating the effects of MBA profile on muscle mechanics

To further understand the muscle-level response, we performed a single-participant study where we collected B-mode ultrasound images of the soleus during walking with and without MBA exosuit across four walking tasks. Our results suggest that the MBA profile resulted in a decrease in the velocity of concentric contraction toward isometric contraction during mid-stance (fig. S4).

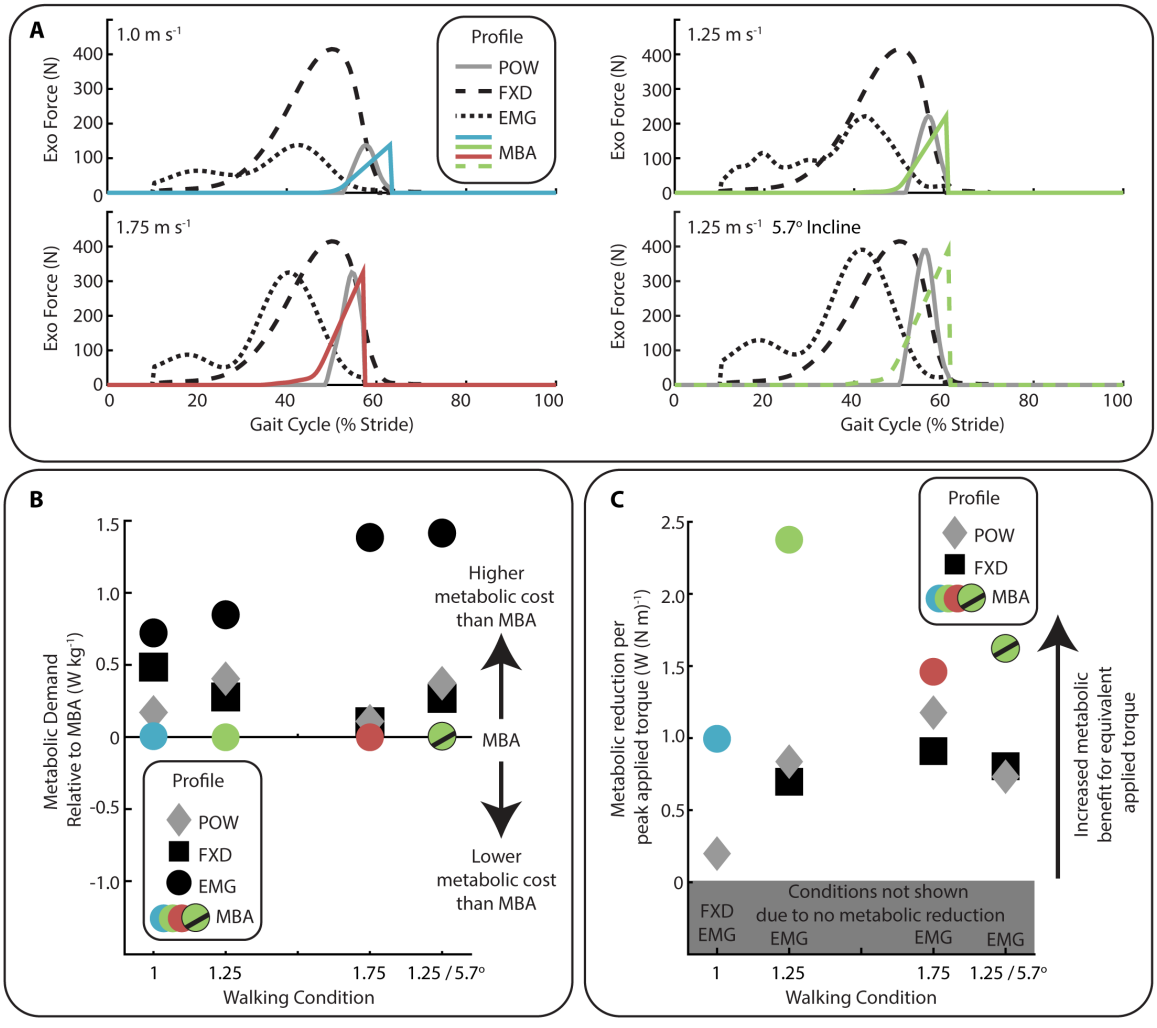

Fig. 4. Direct comparison of MBA to other assistance strategies. For a range of walking speeds and inclines, the effectiveness of the MBA profile was compared with joint power (POW)– and muscle activation (EMG)–based profiles and the average profile from a previous optimization study (FXD). (**A**) The three bioinspired profiles (MBA, EMG, and POW) were generated from the measured biomechanics of the individual for each walking task, whereas the FXD profile was derived from literature. (**B**) The metabolic energy use for each profile relative to the MBA profile. The MBA profile performed better than the POW, EMG, and FXD profiles at reducing metabolic energy use. (**C**) The ratio of the metabolic reduction (watts $kilogram^{-1}$) to the applied ankle assistive torque (newton meter $kilogram^{-1}$). The MBA ankle exosuit had a higher metabolic benefit for equivalent applied torque (n = 2).

Proof of concept: Feasibility of online assistance generation in overground walking

As a proof of concept for real-world use, we demonstrated the feasibility of online adaptive assistance (i.e., capture ultrasound images, process it, and generate a profile) in a mobile version for variable-speed, overground outdoor walking (Supplementary Text, figs. S5 and S6, and movie S1).

DISCUSSION

We have demonstrated that individualized assistance profiles derived directly from measured soleus muscle dynamics can reduce metabolic demand across a range of relevant walking tasks. Although most other studies have tuned and tested for a single walking task, the generalizable MBA approach achieved significant metabolic reductions for three level walking speeds (1.25, 1.5, and 1.75 m s^{-1}) and inclined walking (5.71° at 1.25 m s^{-1}) (Fig. 3D) (*44*). Furthermore, the MBA approach achieved these benefits with relatively low applied force (Fig. 3E and fig. S7).

These reductions in metabolic energy demand were likely partially due to the reduction in soleus activation during mid-late stance (fig. S3 and table S4). Furthermore, our data showed no increase in antagonist TA co-contraction when assistance was applied, which suggests that the MBA approach may have enabled a more "natural" operation in which users did not fight the assistance. TA activity can also help explain the benefit (or lack of benefit) from different levels of assistance at multiple walking speeds (*45*). Participants also significantly increased biological positive ankle power when assistance was applied (fig. S3 and table S2). Although we cannot say from this study, the increase in ankle power may have provided a metabolic benefit by offloading more proximal muscles such as the hip flexors/extensors (*43*, *46*, *47*).

We also aimed to understand the effects of MBA on muscle dynamics. In mid-stance, the MBA profile was likely successful at minimizing the disruption of well-tuned isometric/eccentric contraction. We measured minimal change in ankle dorsiflexion during this period of the gait cycle (fig. S3), which can be an indicator of trained (i.e., effective) exoskeleton use (*48*). Prior studies have shown that exoskeletons for PF assistance can result in decreased dorsiflexion angle, which may lead to decreased MT length and reduced tendon stretch (*49*). Furthermore, in the single-participant study, we measured little to no shift into eccentric contraction velocity, which supports the prediction that tendon energy storage mechanics will be maintained with MBA (fig. S4). Conversely, in late stance, the MBA profile may not have fully achieved the design goal of completely offsetting soleus positive power. Because ankle velocity/power increased, we expect that muscle velocity did not decrease when assistance was applied (fig. S3 and table S2).

Because the MBA strategy was derived from the user's measured muscle mechanics, the assistance profiles changed in sync with the user's muscle mechanics as the walking task changed. The trends in the timing and magnitude of the generated force profiles indicate that our method was able to capture the changes related to the increased muscle force/work demands for faster (*26*, *33*) and inclined walking (Supplementary Text) (*32*, *34*). Although the MBA profile is difficult to parameterize because each time point is uniquely defined using measured muscle velocity, for deeper analysis, we focused on characterizing the assistance onset timing and the peak magnitude, both important and commonly defined parameters for ankle devices (*15*). Other control parameters (e.g., peak timing and offset timing) have also been used for profile generation (*15*) but were not the primary parameters of interest for this work.

The onset of force development for the MBA profiles (Fig. 3A, fig. S2, and table S1) generally falls into what seems to be an important time slot between the early onset times (~10%), associated with torque (*50*) and soleus EMG (*23*) profiles, and the later onset times (~45% at 1.25 and 1.5 m s^{-1}), associated with joint positive power used in other studies (*18*, *19*, *21*). The approaches that assisted earlier in the gait cycle (or assist too much in early-mid stance) often resulted in increased total ankle moment (*23*, *42*, *49*) and may have disrupted normal tuned MT dynamics by unloading the energy that was stored in the tendon while the muscle was still isometric [0% to (*a*) in Fig. 1A]. That additional force then needed to be made up in the latter portion of the gait cycle by increasing muscle contraction, delivering high levels of assistance, or directly or indirectly assisting muscles other than soleus (e.g., hip flexors) (*20*). In our additional study comparing MBA with EMG-based assistance, the EMG profile timing was earlier than MBA, and the MBA profile resulted in lower metabolic demand for all walking tasks (Fig. 4B). Compared with devices that target ankle power, the onset of assistance from our device tended to be earlier. By the time the ankle is producing positive power, the underlying muscle has likely already begun producing positive power. Hence, previous approaches may have missed an opportunity to assist the muscle during the early regions of concentric contraction [(*a*) to (*b*) in Fig. 1A]. In our additional study comparing MBA with a power-based profile (POW), the onset of MBA was earlier than POW, and MBA had better metabolic reductions for all walking tasks (Fig. 4B). As speed and incline increased, the difference in timing between the onset of muscle contraction and joint positive power increased (Fig. 3A, figs. S2 and S3, and table S1), which suggests the importance of measuring and calculating muscle mechanics to adjust assistance as tasks change.

By tailoring assistance to measured MT dynamics from the individual, the MBA profiles can be highly effective at reducing metabolic demand without the need to apply high forces. Compared with the 0.23 N m kg^{-1} average assistance with MBA, other recent ankle devices applied assistance in the range of 0.39 to 0.75 N m kg^{-1} at 1.25 m s^{-1} (fig. S7) (*15*, *37*, *38*, *40*). We directly demonstrated this assistance efficiency in our additional study by comparing MBA against a fixed profile (FXD) that has been proven to be effective at 1.25 m s^{-1} but applies a higher, fixed level of assistance across walking tasks (Fig. 4C) (*15*, *37*). The MBA profile resulted in better metabolic benefit while delivering lower levels of assistance (Fig. 3E). We also showed that too much assistance was detrimental at slow walking speeds, which further suggests that applied assistance may be better informed by muscle mechanics than joint mechanics. Whether a "task-tuned" FXD profile (i.e., not individualized) would perform as well as the MBA profile was unclear because we cannot completely distinguish what portions of the metabolic benefit were from the individualization versus the general characteristics of the profile. We did not try to develop a generic profile for any of the walking tasks because of the large variability in MBA profiles across users. Some of these questions may also be addressed by other studies (*51*).

This ability to achieve metabolic benefit with relatively low forces has implications for exosuit design for long-term, real-world use by allowing for smaller and lighter power sources and actuators, which, in turn, further decreases loading while increasing comfort. In a

proof-of-concept real-world evaluation, we demonstrated online adaptive assistance in a mobile version for variable-speed, overground outdoor walking (Supplementary Text, figs. S5 and S6, and movie S1). Unlike HIL optimization, the assistance profile can be generated with only a few seconds of walking data, making rapid individualization of assistance possible in a wide range of walking scenarios. Combined with the relatively low force requirements, this MBA approach opens up the possibility of real-world application to small mobile devices that are comfortable and work synergistically with the user.

The design goal of the MBA approach was to, at least partially, replace the force produced by the muscle during concentric contraction with exosuit assistance and still allow individuals to walk "normally." Thus, when designing the approach for the MBA profiles, we intentionally derived the assistance profile from the unassisted muscle dynamics. Inherent in this approach was the assumption that as individuals become proficient with the device, they will attempt to walk with joint dynamics that are similar to their normal dynamics (*48*). In addition, we assumed that the muscle dynamics of the individuals would be similar between testing sessions. The alternative would be to measure muscle dynamics while assistance is applied. In this case, even if joint dynamics were unchanged as suggested during mid-stance in our study (fig. S3), the underlying MT dynamics would likely be in an altered state (*49*, *52*). Here, we focused on developing a technique that enabled a reasonably accurate estimate of soleus concentric contraction that could then be applied to developing assistance profiles.

Given the complexity of the plantar flexor MTs, numerous simplifications were used in our development of the MBA exosuit profile. Our goal in this work was to develop a simple and robust method for estimating the force needed to at least partially offset the shortening of the bulk muscle. We briefly discuss this here but provide additional detail on the justification of assumptions/simplifications and their implications in the Supplementary Text. The soleus MT and the interaction of the soleus with the tendon and two parallel gastrocnemius muscles that make up the triceps surae muscle group are complex (*53*, *54*). The free tendon of the AT becomes the aponeurosis as it encapsulates and extends along the length of the muscle (*55*). The displacement of the muscle depends on the location, and the displacement that is measured more proximally is likely greater than the displacement more toward the ankle (free tendon) (*56*). We picked a location over the medial gastrocnemius (MG) because the soleus MT junction is very distal and difficult to measure (particularly with boots), and the location over the MG provided a stable anchor point. The MBA method additionally assumed that the tendon interacted purely in-series with the soleus muscle, a simplification that has been recommended and used in prior models (*57*, *58*). We assumed a constant soleus moment arm similar to prior work modeling the soleus MT (*58*). However, in vivo experiments during walking have found that, although 41 mm is close to the average moment arm throughout the gait cycle, there can be 1 to 2 mm of variation during the mid-late stance phase (*59*). This variation is small and may lead to errors of 2 to 5% in the generated force profiles.

We assumed that ankle dorsiflexion minimally affected the measurement of concentric contraction. This assumption may have led to the underestimation of force produced by the muscle during concentric contraction as dorsiflexion lengthens the MT. During the late-stance phase, because of the rapid movement of the joint and MT, our estimates of muscle contraction were likely less certain. We assumed that muscle contraction velocity was constant during the push-off phase, an approach that is supported by other work that showed a somewhat linear change in muscle length during late stance (*60*).

There are additional limitations related to the metabolic results. We acknowledge that the MBA profile may not be the best assistance for maximizing whole-body metabolic demand. The MBA profile here was designed to target a single muscle/joint and thus does not consider the coordination between joints and muscles. For comparison, HIL optimization often targets whole-body metabolic optimization and may capture some of the interactions across multiple muscles or joints. However, because very few studies are conducted at different walking tasks (*45*, *61*), apart from the additional two-participant study here, we do not have a good comparison of MBA against other approaches for a range of speeds and inclines.

Here, we have demonstrated how users' measured muscle dynamics can be used to develop exosuit assistance profiles that are tailored to the individual and adaptive to dynamic walking tasks. By tuning the assistance to the individuals' muscle mechanics, our MBA strategy provided metabolic benefit in multiple walking tasks using relatively low forces. Thus, the MBA strategy is both effective and efficient. On the basis of the MBA principles presented here, future work may be able to improve estimation methods and closed-loop controllers to enable real-time dynamic control for real-world tasks.

MATERIALS AND METHODS

Participants

Nine healthy adults [n = 9, 3 females and 6 males; age = 29.1 ± 4.04 years (means ± SD); mass = 67.9 ± 12.9 kg; height = 1.71 ± 0.07 m] participated in the study. All participants reported no previous history of musculoskeletal injury or diseases, and all participants provided written informed consent before their participation. The study was approved by the Harvard Longwood Medical Area Institutional Review Board, and all methods were carried out in accordance with the approved study protocol.

Experimental procedure and study design

Overview

All participants attended three experimental visits: a baseline biomechanics assessment, a training visit, and a testing visit. In brief, in the first visit, participants walked without wearing a device while we measured their baseline biomechanics, including muscle mechanics. These data were used to develop user-specific MBA profiles for the different walking tasks, which were then applied back to the participant in the second (training) and the third (testing) visits.

Visit 1—Baseline biomechanics assessment

In the first visit, each participant walked on a treadmill at six different walking tasks: five level ground speeds of 0.75, 1.00, 1.25, 1.5, and 1.75 m s^{-1} and one 5.71° (10%) grade at 1.25 m s^{-1}. Participants walked for 2 min for each task while lower-limb segment motions were measured using a motion capture system (120 Hz; Qualisys, Gothenburg, Sweden), and three-dimensional ground reaction forces (GRFs) were measured by an instrumented treadmill (1200 Hz; Bertec, Columbus, OH, USA). Surface EMG (1200 Hz; Delsys, Natick, MA, USA) captured muscle activation of the soleus and TA. A low-profile ultrasound transducer (113 Hz; MicrUs, Telemed, Vilnius, Lithuania) attached on the left leg over the MG

captured B-mode ultrasound images of the MG and soleus. Participants wore the same shoes during the baseline collection as in the later visits to maintain similar loading conditions. Data from the last 30 s of 0.75 m s^{-1} walking were used to estimate AT quasi-stiffness, as outlined in the "Estimation of AT quasi-stiffness" section, and from the remaining walking conditions to develop the user-specific force profiles for different walking tasks, as outlined in the "B-mode ultrasound-derived assistance profile generation" section.

Visit 2—Training

In the second session, each participant walked for the latter five tasks (1.00, 1.25, 1.5, and 1.75 m s^{-1} and 5.71°) while wearing an active ankle exosuit applying their customized assistance profiles. At the beginning of each task, the participants underwent a procedure for setting the maximum cable retraction limit to prevent overrotation at ankle joints (see "Control approach" in the "Soft exosuit" section for details). Then, the participants walked for 5 to 10 min for each task (5 min for 1.75 m s^{-1} and 5.71°, 10 min for the rest) and experienced walking with the active exosuit using the customized assistance profiles. While walking, the participants were instructed to try to conform to the external assistance and to try not to resist it. For the training session, no measurements were collected.

Visit 3—Testing

In the third session, each participant again walked on a treadmill for the same five walking tasks, once while wearing the active exosuit with the MBA profiles and once without the exosuit (NO-DEVICE). To minimize the sequence effect, the NO-DEVICE conditions were tested first for half the participants, and MBA was tested first for the other half. Within the MBA (or NO-DEVICE) grouping, the order of tasks was not randomized. The order was always 1.00 m s^{-1}, 1.25 m s^{-1}, 1.5 m s^{-1}, 5.71°, and 1.75 m s^{-1}. We did this to minimize the potential for fatigue to affect measurements at the slower speeds, and we determined it suitable because different speed/incline tasks were not directly compared with each other (i.e., active assistance at 1.0 m s^{-1} was not compared with 1.25 m s^{-1}). While participants walked for 5 min in each walking task and suit condition, we measured the metabolic cost of walking by portable indirect calorimetry (K5, COSMED, Rome, Italy), TA and soleus (SOL) muscle activity with EMG (2040 Hz), and lower-limb segment motions and GRFs. We were concerned about participant comfort biasing metabolic measurements and decided to minimize the placement of sensors underneath or near the textile components of the exosuit. Hence, we did not collect EMG data from the gastrocnemius and, similarly, did not collect ultrasound during the active exosuit conditions in the main study.

B-mode ultrasound-derived assistance profile generation

The output of the MBA process was an estimate of how much additional force the soleus muscle contributed to the MT force by concentrically contracting. Our approach calculates the additional soleus force by estimating the stretch the soleus contraction imparts on the in-series AT and then multiplying by the estimated tendon quasi-stiffness (Eq. 1) (fig. S1)

$$F_{\mathrm{SOL\_Conc}} = \Delta L_{\mathrm{SOL/AT}} * k_{\mathrm{AT}} * rPCSA_{\mathrm{SOL}} \quad (1)$$

Although the equation is quite simple, the challenge lies in the inability to easily measure muscle state and tendon physiological properties. In our approach, to calculate the additional stretch that the soleus contraction imparts on the in-series AT by shortening ($\Delta L_{\mathrm{SOL/AT}}$) for each individual and walking task, we measured the soleus contraction velocity and integrated it to estimate the AT stretch. Furthermore, we estimated the AT quasi-stiffness (k_{AT}) for each individual and scaled the resultant force to the approximate contribution of the soleus relative to the plantar flexors ($rPCSA_{\mathrm{SOL}}$ = 0.54) (*36*). Many assumptions and simplifications are built into this approach (see Discussion). Our focus was on developing a technique that enabled a reasonably accurate estimate of soleus concentric contraction that could then be applied to developing assistance profiles.

Direct measurements of muscle kinematics

In the first session, we securely attached a low-profile ultrasound transducer over the left MG, which gave a view of both the MG and the underlying soleus (*49*, *62*). We assumed that MT dynamics would be similar across both legs based on prior work studying the soleus across walking speeds (*33*). With the participant walking on the treadmill, for each speed and incline, we recorded about 10 s of continuous B-mode ultrasound images of the soleus muscle at ~113 Hz during the last 30 s of the trial. The ultrasound image frames were synced with the motion capture and GRF data.

Estimation of soleus contraction velocity and estimation of AT stretch

In postprocessing, we used a custom MATLAB (MathWorks, Natick, MA, USA) optical flow algorithm to calculate the soleus velocity that was parallel with the soleus superficial aponeurosis from the continuous sequence of ultrasound images (*62*). The soleus velocity was segmented into individual strides based on GRF heel-strike timestamps to obtain an average velocity profile. We integrated the positive (i.e., shortening) component of the soleus velocity ($\mathrm{Vel}^{+}_{\mathrm{SOL}}$) over the mid-late stance period based on the intention for assistance to increase over the gait cycle and to provide stability to the assistance profile. To calculate the length change of the muscle during the dorsiflexion phase [$\Delta L_{\mathrm{SOL/AT}}(t)\,|_{\mathrm{DF}}$], we integrated the measured velocity beginning at 20% gait cycle [i.e., $\Delta L_{\mathrm{SOL/AT}}(0.2) = 0$] up to the transition to ankle PF at t^* (Eqs. 2 and 3). During mid-stance, the ankle is slowly dorsiflexing and elongating the MT. This tends to stretch the muscle and create distal displacement of the muscle. Thus, we assumed that any proximal displacement of the muscle during this intermediate time region is not from joint rotation. Rather, we assumed that any proximal displacement in this region was from concentric contraction. In the PF phase, because the measured soleus velocity was heavily affected by rapid ankle PF, we set the velocity to the measured velocity at the transition to PF [i.e., $Vel^{+}_{SOL}(t)\,|_{t\geq t^*} = Vel^{+}_{SOL}(t^*)$]. This approach is supported by other work that showed a somewhat linear change in muscle length during late stance (*60*)

$$t^* = \underset{t}{\mathrm{argmin}}\{Vel_{ANK}(t) > 0 \;\&\; t > 0.2\} \quad (2)$$

$$\Delta L_{\mathrm{SOL/AT}}(t) = \int_{\substack{\text{mid-late}\\ \text{stance}}} Vel^{+}_{SOL}(t)\cdot dt \approx \begin{cases} \int_{0.2}^{t} Vel^{+}_{SOL}(t)\cdot dt \;(0.2 \leq t < t^*) \\ \int_{0.2}^{t^*} Vel^{+}_{SOL}(t)\cdot dt + \int_{t^*}^{t} Vel^{+}_{SOL}(t^*)\cdot dt \;(t^* \leq t < \text{toe-off}) \end{cases} \quad (3)$$

We then combined the two phases sequentially to estimate the length change of the soleus muscle due to concentric contraction throughout stance. Because the soleus and AT are in-series, we assumed that the additional AT stretch due to concentric contraction was equal to the length change of the soleus (i.e., $\Delta L_{\mathrm{SOL/AT}} = -\Delta L_{\mathrm{SOL}} = \Delta L_{\mathrm{AT}}$).

Estimation of AT quasi-stiffness

We estimated the individuals' AT quasi-stiffness (length-tension relationship) (k_{AT}) based on the ankle angle and ankle moment during the mid-late stance while walking slowly (*58*). We assumed that the plantar flexor muscles isometrically contract and do not change their length during this period (i.e., the ankle angle change is associated only with the AT length change), the dorsiflexor muscles are not active during this period (i.e., the ankle moment is associated only with the force on the AT), and the AT quasi-stiffness curve is linear. Thus, we estimated that the ankle's quasi-stiffness during this region was generated from the AT quasi-stiffness. The AT length change and the force on the AT were estimated for 35 to 40% gait cycle from the ankle angle change and the ankle moment during 0.75 m s^{-1} walking, respectively, assuming a constant biological moment arm of the ankle (ma_{ANK} = 0.041 m) (*58*). AT force was estimated by dividing the ankle moment by the assumed moment arm of the biological ankle (ma_{ANK} = 0.041 m) (*58*). We then estimated the AT quasi-stiffness as the slope of a linear regression line between the estimated AT force and AT length. The average R^2 of the linear regression was 0.998, confirming that the linearity assumption was valid.

Generation of assistance profile

We then multiplied the AT stretch profiles for each participant by their estimated AT quasi-stiffness (k_{AT}) and $rPCSA_{SOL}$ (Eq. 1) to generate an estimated biological force generated by the soleus concentric contraction for each task and person (F_{SOL_Conc}). Last, we calculated the exosuit force (F_{EXO}) required to generate an equivalent (and thus offsetting) ankle moment to that generated by the estimated soleus muscle force (F_{SOL_Conc}) by multiplying by the ratio of the assumed moment arm of the biological ankle (ma_{ANK} = 0.041 m) (*58*) and exosuit (ma_{EXO} = 0.10 m) (Eq. 4)

$$F_{EXO} = F_{SOL\_Conc} * \frac{ma_{ANK}}{ma_{EXO}} \quad (4)$$

By providing an equivalent torque, the goal of this method was to offset only the force produced by the muscle during concentric contraction in mid-late stance when the MT dynamics become relatively uneconomical.

Direct comparison of MBA to other assistance profiles

Our direct comparison of MBA against alternative assistance strategies let us better understand how the MBA performed relative to other bioinspired approaches. For two individuals (one male and one female), we performed a direct head-to-head comparison of the MBA profile to other biological mechanism–derived strategies and an average profile based on a previous optimization study (*15*, *37*) in an additional visit. The four assistance profiles were MBA, muscle activation (EMG), ankle positive power (POW), and a fixed literature reference (FXD). We used the participant's data from the first biomechanics visit, which collected baseline soleus EMG, ankle joint dynamics, and B-mode ultrasound of the soleus for walking tasks at 1.0, 1.25, and 1.75 m s^{-1} and 5.71° to develop the assistance profiles. The baseline soleus EMG envelope and positive ankle power profiles calculated in each walking task were used as the assistance profiles for EMG and POW, respectively, and thus, each profile was unique to both the user and the walking task. The peak demanded forces for the MBA, EMG, and POW profiles were set to be the same to allow for a fair comparison across biologically inspired approaches because prior studies have shown that increasing assistance magnitude can increase metabolic benefit (*20*). For FXD, an averaged profile from a previous HIL optimization study (*15*) was used. This reference has been used in other ankle assistive device papers (*37*). The peak magnitude of the averaged ankle moment assistance profile was 0.75 N m kg^{-1}, and the profile was scaled by each participant's body weight (60 and 56 kg, respectively) and the moment arm of the exosuit (ma_{EXO} = 0.10 m).

On the testing day, each participant walked on a treadmill in the order of 1.00 m s^{-1}, 1.25 m s^{-1}, 5.71°, and 1.75 m s^{-1}. We removed the 1.5 m s^{-1} task to maintain the range of tasks while keeping a reasonable session length. The four assistance profiles were applied at each walking task in randomized order. The participant walked for 5 min for each suit condition and walking task, and we measured the metabolic cost of walking with portable indirect calorimetry. A training day was not performed. The two participants had been tested with the MBA profile previously, but because the gap between this and the previous session was 8 months, we determined that training was not a factor.

Soft exosuit

Apparel components

The soft exosuit was designed to assist ankle PF during walking (Fig. 3B). The exosuit textile components per leg consisted of an underlying Fabrifoam liner, a calf wrap, and an arch-shaped rigid plastic shield inserted in between to prevent compression-induced fatigue of the TA muscle. The calf wraps were similar to those previously reported by our group (*18*, *63*) but redistributed the compression toward the most superior region of the shank to permit the calf muscles to bulge in a more physiologically relevant manner while walking (*64*).

Hardware implementation

An offboard actuator with two custom motors (Allied Motion Technologies, Amherst, NY, USA) was used to generate assistive forces (*65*, *66*). Bowden cables between the posterior calves and heels were used to transmit the forces to the user. An inertial measurement unit (IMU; MTi-3 AHRS, Xsens Technologies, Enschede, The Netherlands) on each foot and a load cell (LSB200, FUTEK Advanced Sensor Technology, Irvine, CA, USA) on each calf wrap were used to track and apply assistance. All components on both legs had a total mass of 0.68 kg.

Control approach

A real-time target machine (Speedgoat, Liebefeld, Switzerland) ran a custom Simulink (MathWorks, Natick, MA, USA) model to drive the motors in the offboard actuator. The high-level controller in the Simulink model was designed to generate the desired force profiles over a gait cycle while not rotating the ankle joints excessively. First, the controller detected heel strikes for each leg using the foot IMU and segmented walking cycles (*21*). Then, the controller ran a PI force control loop cascaded with a current loop to track the desired force profile (*66*). While running the force control loop, the controller also monitored the Bowden cable retraction length and released the cable as soon as the motor reached a participant/task-specific maximum retraction threshold. For this, at the beginning of each active exosuit condition, a handheld controller was used to allow the participant to set the cable retraction threshold as high as possible while ensuring that the assistance did not overrotate their ankles. This approach enabled safe and robust force tracking until the end of push-off.

Data analysis

Analog GRF data and marker positions were filtered at 10 Hz. For identifying t^* only, we separately filtered marker positions for kinematics at 20 Hz. We performed inverse dynamics analysis to calculate the left leg total joint moments and powers (Visual3D, C-Motion, Germantown, MD, USA). Exosuit torque was calculated by multiplying the exosuit force measured by load cells by the exosuit moment arm. Exosuit moment arm was dynamic and calculated for the entire stride as the perpendicular distance between the joint center and line between markers on either end of the exposed inner Bowden cable (boot attachment and calf wrap). The biological contribution to the total ankle joint moment was calculated by subtracting the calculated exosuit torque from the total ankle moment. Joint angles and moments were reported for the sagittal plane. To calculate the EMG linear envelope, the raw EMG was band-pass filtered at 20 to 450 Hz, rectified, and low-pass filtered at 10 Hz. The amplitude of the EMG envelope for each muscle was normalized to the peak amplitude for that muscle measured across all walking tasks and suit conditions for each participant. For each participant, suit condition, and walking task, the joint mechanics and muscle activation data were segmented by heel strikes, time-normalized, and averaged to generate average time-normalized metrics. For the summary statistics, average data (e.g., average moment) were the time integral of the time series data divided by the time period. Average data for particular phases of a stride were computed as the time integral over that phase divided by the time elapsed during that gait phase.

Statistics

For net metabolic power, joint dynamics, and EMG, we reported the means and SEs calculated across participants. The MBA profile was statistically evaluated against NO-DEVICE at each walking task independently (JMP Pro, SAS Institute, Cary, NC, USA). In the evaluation of the effectiveness of the assistance profile, no statistical comparison was made across different walking tasks. For metrics where data were normally distributed, we used a paired t test to compare MBA with NO-DEVICE ($\alpha = 0.05$). Net metabolic data were not normally distributed, and we applied the Wilcoxon signed-rank, two-tailed test ($\alpha = 0.05$). Two individuals were unable to complete fast walking (1.75 m s^{-1}), and we report the actual sample size in the results and within figure captions ($n = 7$). Joint mechanics and EMG data were unusable for some other conditions because of noise or treadmill belt crossovers, and we report the actual sample size next to the data. No statistical analysis was performed for the additional studies because of the small sample size.

SUPPLEMENTARY MATERIALS

www.science.org/doi/10.1126/scirobotics.abj1362
Text
Figs. S1 to S7
Tables S1 to S5
Data file S1
Movie S1
References (*68*–*76*)

REFERENCES AND NOTES

1. R. W. Bohannon, Comfortable and maximum walking speed of adults aged 20-79 years: Reference values and determinants. *Age Ageing* **26**, 15–19 (1997).
2. M. M. Samson, A. Crowe, P. L. de Vreede, J. A. G. Dessens, S. A. Duursma, H. J. J. Verhaar, Differences in gait parameters at a preferred walking speed in healthy subjects due to age, height and body weight. *Aging Clin. Exp. Res.* **13**, 16–21 (2001).
3. E. Mattsson, U. Evers Larsson, S. Rössner, Is walking for exercise too exhausting for obese women? *Int. J. Obes.* **21**, 380–386 (1997).
4. R. C. Browning, E. A. Baker, J. A. Herron, R. Kram, Effects of obesity and sex on the energetic cost and preferred speed of walking. *J. Appl. Physiol.* **100**, 390–398 (2006).
5. D. Malatesta, D. Simar, Y. Dauvilliers, R. Candau, F. Borrani, C. Préfaut, C. Caillaud, Energy cost of walking and gait instability in healthy 65- and 80-yr-olds. *J. Appl. Physiol.* **95**, 2248–2256 (2003).
6. R. M. Guimaraes, B. Isaacs, Characteristics of the gait in old people who fall. *Disabil. Rehabil.* **2**, 177–180 (1980).
7. S. L. Patterson, L. W. Forrester, M. M. Rodgers, A. S. Ryan, F. M. Ivey, J. D. Sorkin, R. F. Macko, Determinants of walking function after stroke: Differences by deficit severity. *Arch. Phys. Med. Rehabil.* **1**, 115–119 (2007).
8. D. Tan, M. Danoudis, J. McGinley, M. E. Morris, Relationships between motor aspects of gait impairments and activity limitations in people with Parkinson's disease: A systematic review. *Parkinsonism Relat. Disord.* **18**, 117–124 (2012).
9. R. L. Knoblauch, M. T. Pietrucha, M. Nitzburg, Field studies of pedestrian walking speed and start-up time. *Transp. Res. Rec.* **1**, 27–38 (1996).
10. R. Rastogi, I. Thaniarasu, S. Chandra, Design implications of walking speed for pedestrian facilities. *J. Transp. Eng.* **137**, 687–696 (2011).
11. F. A. Panizzolo, S. Lee, T. Miyatake, D. M. Rossi, C. Siviy, J. Speeckaert, I. Galiana, C. J. Walsh, Lower limb biomechanical analysis during an unanticipated step on a bump reveals specific adaptations of walking on uneven terrains. *J. Exp. Biol.* **220**, 4169–4176 (2017).
12. C. M. Wall-Scheffler, Sex differences in incline-walking among humans. *Integr. Comp. Biol.* **55**, 1155–1165 (2015).
13. D. J. Farris, G. S. Sawicki, The mechanics and energetics of human walking and running: A joint level perspective. *J. R. Soc. Interface* **9**, 110–118 (2012).
14. J. R. Montgomery, A. M. Grabowski, The contributions of ankle, knee and hip joint work to individual leg work change during uphill and downhill walking over a range of speeds. *R. Soc. Open Sci.* **5**, 180550 (2018).
15. J. Zhang, P. Fiers, K. A. Witte, R. W. Jackson, K. L. Poggensee, C. G. Atkeson, S. H. Collins, Human-in-the-loop optimization of exoskeleton assistance during walking. *Science* **356**, 1280–1284 (2017).
16. Y. Ding, M. Kim, S. Kuindersma, C. J. Walsh, Human-in-the-loop optimization of hip assistance with a soft exosuit during walking. *Sci. Robot.* **3**, eaar5438 (2018).
17. K. A. Witte, P. Fiers, A. L. Sheets-Singer, S. H. Collins, Improving the energy economy of human running with powered and unpowered ankle exoskeleton assistance. *Sci. Robot.* **5**, eaay9108 (2020).
18. S. Lee, J. Kim, L. Baker, A. Long, N. Karavas, N. Menard, I. Galiana, C. J. Walsh, Autonomous multi-joint soft exosuit with augmentation-power-based control parameter tuning reduces energy cost of loaded walking. *J. Neuroeng. Rehabil.* **15**, 66 (2018).
19. L. M. Mooney, E. J. Rouse, H. M. Herr, Autonomous exoskeleton reduces metabolic cost of human walking. *J. Neuroeng. Rehabil.* **11**, article no. 151 (2014).
20. B. T. Quinlivan, S. Lee, P. Malcolm, D. M. Rossi, M. Grimmer, C. Siviy, N. Karavas, D. Wagner, A. Asbeck, I. Galiana, C. J. Walsh, Assistance magnitude versus metabolic cost reductions for a tethered multiarticular soft exosuit. *Sci. Robot.* **2**, eaah4416 (2017).
21. S. Lee, S. Crea, P. Malcolm, I. Galiana, A. Asbeck, C. Walsh, Controlling negative and positive power at the ankle with a soft exosuit, in *Proceedings of the 33rd IEEE International Conference on Robotics and Automation (ICRA)*, Stockholm, Sweden, 16 to 21 May 2016, pp. 3509–3515.
22. M. Grimmer, B. T. Quinlivan, S. Lee, P. Malcolm, D. M. Rossi, C. Siviy, C. J. Walsh, Comparison of the human-exosuit interaction using ankle moment and ankle positive power inspired walking assistance. *J. Biomech.* **83**, 76–84 (2019).
23. J. R. Koller, D. A. Jacobs, D. P. Ferris, C. D. Remy, Learning to walk with an adaptive gain proportional myoelectric controller for a robotic ankle exoskeleton. *J. Neuroeng. Rehabil.* **12**, 97 (2015).
24. K. Z. Takahashi, M. D. Lewek, G. S. Sawicki, A neuromechanics-based powered ankle exoskeleton to assist walking post-stroke: A feasibility study. *J. Neuroeng. Rehabil.* **12**, 23 (2015).
25. T. J. Roberts, R. L. Marsh, P. G. Weyand, C. R. Taylor, Muscular force in running turkeys: The economy of minimizing work. *Science* **275**, 1113–1115 (1997).
26. D. J. Farris, G. S. Sawicki, Human medial gastrocnemius force-velocity behavior shifts with locomotion speed and gait. *Proc. Natl. Acad. Sci. U.S.A.* **109**, 977–982 (2012).
27. M. Ishikawa, P. V. Komi, M. J. Grey, V. Lepola, G.-P. Bruggemann, Muscle-tendon interaction and elastic energy usage in human walking. *J. Appl. Physiol.* **99**, 603–608 (2005).
28. R. M. Alexander, Optimum muscle design for oscillatory movements. *J. Theor. Biol.* **184**, 253–259 (1997).
29. A. V. Hill, The heat of shortening and the dynamic constants of muscle. *Proc. R. Soc. Lond. Ser. B Biol. Sci.* **126**, 136–195 (1938).
30. T. W. Ryschon, M. D. Fowler, R. E. Wysong, A.-R. Anthony, R. S. Balaban, Efficiency of human skeletal muscle in vivo: Comparison of isometric, concentric, and eccentric muscle action. *J. Appl. Physiol.* **83**, 867–874 (1997).
31. E. M. Arnold, S. R. Hamner, A. Seth, M. Millard, S. L. Delp, How muscle fiber lengths and velocities affect muscle force generation as humans walk and run at different speeds. *J. Exp. Biol.* **216**, 2150–2160 (2013).

32. N. T. Pickle, A. M. Grabowski, A. G. Auyang, A. K. Silverman, The functional roles of muscles during sloped walking. *J. Biomech.* **49**, 3244–3251 (2016).
33. A. Lai, G. A. Lichtwark, A. G. Schache, Y. C. Lin, N. A. Brown, M. G. Pandy, In vivo behavior of the human soleus muscle with increasing walking and running speeds. *J. Appl. Physiol.* **118**, 1266–1275 (2015).
34. G. S. Sawicki, D. P. Ferris, Mechanics and energetics of incline walking with robotic ankle exoskeletons. *J. Exp. Biol.* **212**, 32–41 (2009).
35. T. J. Roberts, The integrated function of muscles and tendons during locomotion. *Comp. Biochem. Physiol. A Mol. Integr. Physiol.* **133**, 1087–1099 (2002).
36. T. Fukunaga, R. R. Roy, F. G. Shellock, J. A. Hodgson, M. K. Day, P. L. Lee, H. Kwong-Fu, V. R. Edgerton, Physiological cross-sectional area of human leg muscles based on magnetic resonance imaging. *J. Orthop. Res.* **10**, 928–934 (1992).
37. R. W. Jackson, S. H. Collins, Heuristic-based ankle exoskeleton control for co-adaptive assistance of human locomotion. *IEEE Trans. Neural Syst. Rehabil. Eng.* **10**, 2059–2069 (2019).
38. G. S. Sawicki, D. P. Ferris, Powered ankle exoskeletons reveal the metabolic cost of plantar flexor mechanical work during walking with longer steps at constant step frequency. *J. Exp. Biol.* **212**, 21–31 (2009).
39. P. Malcolm, W. Derave, S. Galle, D. De Clercq, A simple exoskeleton that assists plantarflexion can reduce the metabolic cost of human walking. *PLOS ONE* **8**, e56137 (2013).
40. S. Galle, P. Malcolm, S. H. Collins, D. De Clercq, Reducing the metabolic cost of walking with an ankle exoskeleton: Interaction between actuation timing and power. *J. Neuroeng. Rehabil.* **14**, 35 (2017).
41. C. Khazoom, C. Veronneau, J. P. L. Bigue, J. Grenier, A. Girard, J. S. Plante, Design and control of a multifunctional ankle exoskeleton powered by magnetorheological actuators to assist walking, jumping, and landing. *IEEE Robot. Autom. Lett.* **4**, 3083–3090 (2019).
42. S. H. Collins, M. B. Wiggin, G. S. Sawicki, Reducing the energy cost of human walking using an unpowered exoskeleton. *Nature* **522**, 212–215 (2015).
43. L. M. Mooney, H. M. Herr, Biomechanical walking mechanisms underlying the metabolic reduction caused by an autonomous exoskeleton. *J. Neuroeng. Rehabil.* **13**, 4 (2016).
44. G. S. Sawicki, O. N. Beck, I. Kang, A. J. Young, The exoskeleton expansion: Improving walking and running economy. *J. Neuroeng. Rehabil.* **17**, 25 (2020).
45. R. W. Nuckols, G. S. Sawicki, Impact of elastic ankle exoskeleton stiffness on neuromechanics and energetics of human walking across multiple speeds. *J. Neuroeng. Rehabil.* **17**, 75 (2020).
46. C. L. Lewis, D. Ferris, Walking with increased ankle pushoff decreases hip muscle moments. *J. Biomech.* **41**, 2082–2089 (2008).
47. S. N. Fickey, M. G. Browne, J. R. Franz, Biomechanical effects of augmented ankle power output during human walking. *J. Exp. Biol.* **221**, 182113 (2018).
48. K. E. Gordon, D. P. Ferris, Learning to walk with a robotic ankle exoskeleton. *J. Biomech.* **40**, 2636–2644 (2007).
49. R. W. Nuckols, T. J. M. Dick, O. N. Beck, G. S. Sawicki, Ultrasound imaging links soleus muscle neuromechanics and energetics during human walking with elastic ankle exoskeletons. *Sci. Rep.* **10**, 3604 (2020).
50. R. W. Jackson, S. H. Collins, An experimental comparison of the relative benefits of work and torque assistance in ankle exoskeletons. *J. Appl. Physiol.* **119**, 541–557 (2015).
51. K. L. Poggensee, S. H. Collins, How adaptation, training, and customization contribute to benefits from exoskeleton assistance. *bioRxiv* 2021.04.25.440289 (2021).
52. R. W. Jackson, C. L. Dembia, S. L. Delp, S. H. Collins, Muscle-tendon mechanics explain unexpected effects of exoskeleton assistance on metabolic rate during walking. *J. Exp. Biol.* **220**, 2082–2095 (2017).
53. T. Finni, J. A. Hodgson, A. M. Lai, V. R. Edgerton, S. Sinha, Mapping of movement in the isometrically contracting human soleus muscle reveals details of its structural and functional complexity. *J. Appl. Physiol.* **95**, 2128–2133 (2003).
54. J. A. Hodgson, T. Finni, A. M. Lai, V. R. Edgerton, S. Sinha, Influence of structure on the tissue dynamics of the human soleus muscle observed in MRI studies during isometric contractions. *J. Morphol.* **267**, 584–601 (2006).
55. E. Azizi, G. M. Halenda, T. J. Roberts, Mechanical properties of the gastrocnemius aponeurosis in wild turkeys. *Integr. Comp. Biol.* **1**, 51–58 (2009).
56. T. Finni, J. A. Hodgson, A. M. Lai, V. R. Edgerton, S. Sinha, Nonuniform strain of human soleus aponeurosis-tendon complex during submaximal voluntary contractions in vivo. *J. Appl. Physiol.* **2**, 829–837 (2003).
57. F. E. Zajac, Muscle and tendon: Properties, models, scaling, and application to biomechanics and motor control. *Crit. Rev. Biomed. Eng.* **17**, 359–411 (1989).
58. G. S. Sawicki, N. S. Khan, A simple model to estimate plantarflexor muscle-tendon mechanics and energetics during walking with elastic ankle exoskeletons. *IEEE Trans. Biomed. Eng.* **63**, 914–923 (2016).
59. K. Rasske, D. G. Thelen, J. R. Franz, Variation in the human Achilles tendon moment arm during walking. *Comput. Methods Biomech. Biomed. Eng.* **20**, 201–205 (2017).
60. J. Rubenson, N. J. Pires, H. O. Loi, G. J. Pinniger, D. G. Shannon, On the ascent: The soleus operating length is conserved to the ascending limb of the force-length curve across gait mechanics in humans. *J. Exp. Biol.* **215**, 3539–3551 (2012).
61. J. Kim, G. Lee, R. Heimgartner, D. A. Revi, N. Karavas, D. Nathanson, I. Galiana, A. Eckert-Erdheim, P. Murphy, D. Perry, N. Menard, D. K. Choe, P. Malcolm, C. J. Walsh, Reducing the metabolic rate of walking and running with a versatile, portable exosuit. *Science* **365**, 668–672 (2019).
62. R. W. Nuckols, K. Swaminathan, S. Lee, L. Awad, C. J. Walsh, R. D. Howe, Automated detection of soleus concentric contraction in variable gait conditions for improved exosuit control, in *Proceeding of the 2020 IEEE International Conference on Robotics and Automation (ICRA)*, Paris, France, 31 May to 31 August 2020, pp. 4855–4862.
63. S. Lee, N. Karavas, B. T. Quinlivan, D. LouiseRyan, D. Perry, A. Eckert-Erdheim, P. Murphy, T. G. Goldy, N. Menard, M. Athanassiu, J. Kim, G. Lee, I. Galiana, C. J. Walsh, Autonomous multi-joint soft exosuit for assistance with walking overground, in *Proceeding of the IEEE International Conference on Robotics and Automation (ICRA)*, Brisbane, QLD, Australia, 21 to 25 May 2018, pp. 2812–2819.
64. E. Azizi, E. L. Brainerd, T. J. Roberts, Variable gearing in pennate muscles. *Proc. Natl. Acad. Sci. U.S.A.* **105**, 1745–1750 (2008).
65. G. Lee, Y. Ding, I. G. Bujanda, N. Karavas, Y. M. Zhou, C. J. Walsh, Improved assistive profile tracking of soft exosuits for walking and jogging with off-board actuation, in *Proceedings of the IEEE/RSJ International Conference on Intelligent Robots and Systems (IROS)*, Vancouver, BC, Canada, 24 to 28 September 2017, pp. 1699–1706.
66. M. Kim, C. Liu, J. Kim, S. Lee, A. Meguid, C. J. Walsh, S. Kuindersma, Bayesian optimization of soft exosuits using a metabolic estimator stopping process, in *Proceedings of the International Conference on Robotics and Automation (ICRA)*, Montreal, QC, Canada, 20 to 24 May 2019, pp. 9173–9179.
67. L. M. Mooney, E. J. Rouse, H. M. Herr, Autonomous exoskeleton reduces metabolic cost of human walking during load carriage. *J. Neuroeng. Rehabil.* **11**, article no. 80 (2014).
68. G. A. Lichtwark, A. M. Wilson, In vivo mechanical properties of the human Achilles tendon during one-legged hopping. *J. Exp. Biol.* **208**, 4715–4725 (2005).
69. G. L. Onambele, M. V. Narici, C. N. Maganaris, Calf muscle-tendon properties and postural balance in old age. *J. Appl. Physiol.* **100**, 2048–2056 (2006).
70. K. C. Moisio, D. R. Sumner, S. Shott, D. E. Hurwitz, Normalization of joint moments during gait: A comparison of two techniques. *J. Biomech.* **36**, 599–603 (2003).
71. D. J. Farris, G. A. Lichtwark, UltraTrack: Software for semi-automated tracking of muscle fascicles in sequences of B-mode ultrasound images. *Comput. Methods Prog. Biomed.* **128**, 111–118 (2016).
72. E. Azizi, T. J. Roberts, Biaxial strain and variable stiffness in aponeuroses. *J. Physiol.* **587**, 4309–4318 (2009).
73. T. J. M. Dick, A. S. Arnold, J. M. Wakeling, Quantifying Achilles tendon force in vivo from ultrasound images. *J. Biomech.* **49**, 3200–3207 (2016).
74. G. A. Lichtwark, A. M. Wilson, Interactions between the human gastrocnemius muscle and the Achilles tendon during incline, level and decline locomotion. *J. Exp. Biol.* **209**, 4379–4388 (2006).
75. N. J. Cronin, B. I. Prilutsky, G. A. Lichtwark, H. Maas, Does ankle joint power reflect type of muscle action of soleus and gastrocnemius during walking in cats and humans? *J. Biomech.* **46**, 1383–1386 (2013).
76. E. M. Arnold, S. R. Ward, R. L. Lieber, S. L. Delp, A model of the lower limb for analysis of human movement. *Ann. Biomed. Eng.* **38**, 269–279 (2010).

Acknowledgments: We thank A. Eckert-Erdheim, B. Quinlivan, P. Murphy, A. Cantaloube, D. A. Revi, J. Kim, D. Perry, L. Schumm, N. Menard, A. Degirmenci, and S. Sullivan for contributions to this work. **Funding:** This work was supported by NIH grants BRG-R01HD088619, U01TR002775, and R21AR076686; NSF grant CMMI-1925085; Harvard University John A. Paulson School of Engineering and Applied Sciences; Wyss Institute for Biologically Inspired Engineering; Samsung Scholarship; and NSF Graduate Research Fellowship. **Author contributions:** R.W.N., S.L., K.S., R.D.H., and C.J.W. designed the overall concept of the sensing approach and research. R.W.N., S.L., K.S., and C.J.W. designed the overall approach to the exosuit research. R.W.N., S.L., and K.S. developed the sensing and measurement technique. R.W.N., S.L., K.S., and D.O. designed the ankle exosuit. R.W.N., S.L., and K.S. developed the controllers. R.W.N., S.L., and K.S. conducted the experiments. R.W.N., S.L., and K.S. analyzed the data. R.W.N., S.L., K.S., R.D.H., and C.J.W. prepared the manuscript. All authors revised and approved the final manuscript. **Competing interests:** Patents describing the exosuit components documented here have been filed with the U.S. Patent Office. C.J.W. and S.L. are inventors of at least one of the following patent/patent applications: U.S. 9,351,900, U.S. 14/660,704, U.S. 15/097,744, U.S. 14/893,934, PCT/US2014/068462, PCT/US2015/051107, PCT/US2017/042286, U.S. 10,434,030, U.S. 10,843,332, and U.S. 10,427,293 filed by Harvard University. Harvard University has entered into a licensing and collaboration agreement with ReWalk Robotics. C.J.W. is a paid consultant for ReWalk Robotics. The other authors declare that they have no competing interests. **Data and materials availability:** All data needed to support the conclusions of this manuscript are included in the main text or Supplementary Materials. Source data are available in the Supplementary Materials.

Submitted 22 April 2021
Accepted 7 October 2021
Published 10 November 2021
10.1126/scirobotics.abj1362

Science Robotics

Individualization of exosuit assistance based on measured muscle dynamics during versatile walking

R. W. NuckolsS. LeeK. SwaminathanD. OrzelR. D. HoweC. J. Walsh

Sci. Robot., 6 (60), eabj1362. • DOI: 10.1126/scirobotics.abj1362

Science Robotics (ISSN) is published by the American Association for the Advancement of Science. 1200 New York Avenue NW, Washington, DC 20005. The title *Science Robotics* is a registered trademark of AAAS.